Available online at www.sciencedirect.com
ScienceDirect
Journal of the European Ceramic Society 28 (2008) 1769–1776
www.elsevier.com/locate/jeurceramsoc

Light weight silica tiles through foam casting method

Sarika Mishra [a], R. Mitra [b,*], M. Vijayakumar [a]

[a] *Defence Metallurgical Research Laboratory, P.O. Kanchanbagh, Hyderabad 500 058, India*
[b] *Indian Institute of Technology, Kharagpur 721 302, India*

Received 18 July 2007; received in revised form 23 November 2007; accepted 9 December 2007
Available online 4 March 2008

Abstract

The possibility of making porous silica tiles starting from inexpensive fused silica powder using a direct foaming process has been examined. Aqueous slurry of silica with appropriate surfactants and binders have been allowed to foam by entraining air, following which it was cast, dried, and subsequently sintered at 1100 °C. The role of slurry composition and foaming duration, on the green and final density of foams has been studied. Silica foams with density as low as 11% of the theoretical density, and containing interconnected, primarily spherical pores with average size in the range of 50–2000 μm have been fabricated. The porous silica with densities between 18% and 62% of the theoretical value, have shown Young's modulus and compressive strengths in the range of 120–380 MPa and 0.5–3.3 MPa, respectively. A surface densification process, that can seal off the surface pores and provide a smooth exterior to the tiles, has also been established.

Keywords: A. Sintering; Drying; B. Microstructure-final; C. Strength; D. SiO_2

1. Introduction

Amorphous silica has been traditionally used in the components for transient, high temperature structural applications in view of its low density, high melting point, and excellent thermal shock resistance. However, silica is a brittle material with low strength. Hence, instead of monolithic silica, fibrous silica based components with higher toughness have found more applications. One of the most important usages of amorphous silica fibers is in the tiles made for protection of the space shuttle body. The silica fibers used for making these tiles are made either by leaching of high quality glass fibers using a tedious and environmentally unfriendly process, or by drawing from fused quartz melts which increases the cost of fibers. Hence, a different approach involving the application of a foam casting route for fabricating the protective tiles using the amorphous silica powder instead of fibers has attracted considerable attention in recent years. Usage of such an approach for making macroporous ceramic materials, does not compromise the desirable property requirements, and has been reported extensively in the literature.[1–15] Sepulveda[1] and Saggio-Woyansky et al.[2] have reviewed several methods of producing porous alumina ceramics. The patents filed include those describing the use of an air blowing method at high temperatures in clay particles (Sundermann and Viedt),[3] polymeric sponge method (Wood et al.),[4] room temperature atmospheric pressure process (Motoki),[5] froth formation process (Jackson and Meredith),[6] and a chemical reaction based process involving foaming through the evolution of hydrogen gas (Helferich and Schenck).[7] Porous ceramics of various chemical compositions have been produced by Minnear,[8] and Evans and co-workers,[9–11] using some of the methods described above. Recently, Colombo and co-workers[12–14] have developed a method, in which the ceramic particles are replaced by pre-ceramic silicon based polymers, enabling the production of porous ceramics based on amorphous SiC, SiOC, or SiCN with attractive high temperature mechanical properties. Studart et al.[15] have recently provided a comprehensive overview of the methodologies, along with a detailed examination of the underlying principles.

The total porosity in the foam is proportional to the amount of air incorporated into the suspension in the liquid medium during the foaming process. Wet foams are thermodynamically unstable systems, and can easily get destabilized. The main destabilization mechanisms encountered are sedimentation of the slurry, slow growth of air bubble size through Ostwald ripening or coalescence, and subsequent collapse. The size distribution of air

* Corresponding author.
E-mail address: rahul@metal.iitkgp.ernet.in (R. Mitra).

0955-2219/$ – see front matter © 2008 Elsevier Ltd. All rights reserved.
doi:10.1016/j.jeurceramsoc.2007.12.030

bubbles in the foam is affected by the surface tension, which promotes growth in size, so as to decrease the surface area to volume ratio. The increase in the size of incorporated bubbles results in a wide distribution of pores in the final cellular microstructure. It is possible to retard the growth of bubbles, and their collapse by increasing the viscosity of the medium, and kinetically stabilize the foam.[16–19] It is essential that the foams thus made must be stable for time periods long enough to permit removal of the solvent by drying, without affecting the overall porosity and integrity of the cast shape. This paper presents the results of a study on the processing–structure–property relationship of porous silica tiles, prepared by foam casting method using the amorphous silica powder as raw material. In the present study, the effect of slurry composition including the extent of solid loading and binder content, and various process variables such as duration of foaming operation, and rate of drying, on the pore-structure and properties of silica tiles have been examined. The primary objective was to arrive at the optimum process parameters to obtain silica foams with desirable porosity, pore size distribution, strength, and structural integrity.

2. Experimental procedure

2.1. Raw materials

The raw materials used in the study include fused silica powder (Universal Fused Quartz, Bangalore, mean particle size = 10 μm), alumina powder (mean particle size ≅ 0.70 μm and surface area ≅ 7 m^2/g, CT 3000 SG, Alcoa-ACC Industrial Chemicals, Kolkata), cetyl trimethyl ammonium bromide abbreviated later as CTAB (98% pure, chemical reagent grade, S.D. Fine Chemicals Ltd.) as cationic dispersant, and polyvinyl alcohol (PVA, molecular wt. = 1,25,000, Fischer, LR), sucrose (mol. wt. = 342.30, Laboratory Reagent, S.D. Fine Chemicals Ltd.), colloidal silica (mol. wt. = 60.08, pH 8.8, particle size ≅ 27.3 nm, zeta potential ≅ 46.7 mV, silica content = 40%), or aluminium phosphate as binders.

2.2. Foam casting

The processing of silica foams was carried out by carefully following several steps as follows. The first step in foam casting was ball milling of the fused silica powder with 5 wt.% alumina and 0.05% CTAB for 100 h using alumina milling media. Alumina balls of 8–10 mm diameter were used as milling media in 1:1 powder-to-media ratio. Alumina powder was added to inhibit the devitrification of fused silica glass, which otherwise forms cristoballite, giving rise to internal stresses on sintering. This ball-milled powder mixture was used for processing of the silica foams.

The second step involved the preparation of a suspension of silica in aqueous medium by pot milling the constituents at 30 rpm speed in closed polypropylene containers for 2 h. The green strength of the foams was optimized through careful selection of solid loading in the range of 25–35%, binder constituents including 2–4 vol.% PVA, 10–30 vol.% sucrose, as well as 5 vol.% colloidal silica in various combinations. To arrive at the optimum solid loading, and the time used for pot milling operation, separate trials involving mixing of varying amounts of hydrophobic silica powder, water and binders using alumina balls in plastic containers on a roller mill, were carried out to arrive at the optimum solid loading regime. Based on such trial studies, it was found that the compositions containing solid particles occupying 25–35% of the volume give kinetically stable foams. Furthermore, it was found that a homogeneous and viscous slurry forms in about 2 h of mixing.

The third step comprised the foaming operation. The milled slurry was visually examined for smooth flow inside a bottle, which was then put on the roller mill operated at a speed of 30 rpm, and subjected to foaming for 2–4 h by entraining air into the suspension. In addition, orientation of the bottle in the roller mill was repeatedly changed to a position orthogonal with respect to the previous, so that the slurry could move along the length of the bottle and access a larger volume of air. During this step referred to as tumbling, the slurry entrains air far more efficiently and foams. A ratio of 1:3 was maintained for volume of the slurry to that of the container, in order to ensure adequate air entrainment.

In the fourth and fifth steps, the foamed suspensions were aged at room temperature for 10–15 min for foam stabilization, and then cast into suitable petroleum jelly coated rectangular perspex moulds of 10 cm × 10 cm × 4 cm size, respectively. During casting, the mould was periodically tapped to distribute the foam uniformly. The sixth step involved controlled drying of the cast foams. The cast samples were initially dried under controlled condition (T = 30 °C, relative humidity = 40–80%, Osworld Humidity Chamber with accuracy level of temperature and relative humidity as ±0.1 °C and ±3%, respectively) in a graded fashion, followed by drying in a convection oven at temperatures up to 100 °C in steps. Once the free moisture content of the sample attained equilibrium with that of the chamber at a specific temperature, the humidity was lowered further to enhance the drying rate. Optimum drying occurred on holding at 50 °C for 2 h in the hot air oven, followed by that at 80 and 100 °C. In the seventh and final step, the fully dried samples were subjected to binder burn-out followed by sintering at 1100 °C, which was reached at a heating rate of 1 °C/min. Thermogravimetric analysis carried out to monitor the change in mass due to binder burn-out, evaporation or loss of volatile products has shown a mass loss of 12%.

The sample surface obtained by foaming and drying leaves the pore cell walls exposed. In order to prevent them from erosion during handling and usage, the surface needs to be densified and strengthened. For this purpose, a silica slurry with very low solid loading was prepared in aqueous medium with guar gum (0.2–0.5 wt.%) and colloidal silica (5 vol.%) as binder, using 100 h milled precursor powder with particle size of 0.8 μm. The slurry was thoroughly mixed for 24 h, and then applied as a thin coating on all surfaces of the porous green body having dimension of 100 mm × 100 mm × 25 mm. The coated sample was slowly dried up to 110 °C in an air oven. The surface densified and dried porous silica tile thus prepared was sintered at 1100 °C.

2.3. Characterization

Particle size of the pretreated powder was measured using a Zeta Sizer (Model No. 3000 HSA, Malvern Instruments Ltd., UK). A rheometer (Brookfield Rheo 200, Version 2.5) equipped with a vane-shaped spindle was used to characterize rheological behavior of the suspensions in a controlled shear rate mode. The samples were characterized for their green and sintered density by the Archimedes principle, using kerosene (density = 0.798 g/cc) as the liquid being displaced. The microstructure of ceramic foams was characterized quantitatively through optical microscopy, using the image analysis software (Image Tool, version 3.0). In addition, the pore size distribution was characterized through mercury porosimetry (Quantachrome Poremaster, version 4.01, Hg contact angle 140°).

The porous silica foam samples were extremely fragile to handle in green stage as well as in sintered condition. Hence the preparation of samples of specific shapes and sizes involved resin impregnation of the sintered foam samples followed by drying at 60 °C, and curing at 130 °C for 5 min, so that the samples could be handled without breakage. The resin was burnt off after cutting or machining of the samples into desired shapes and sizes. The room temperature air permeability of the sintered disks with 25 mm × 25 mm × 8 mm size was determined by measuring the pressure drop across the sample as a function of the gas flow rate.

For compression tests, the resin-impregnated samples were drilled using ultrasonic drilling machine to obtain cylindrical samples having the dimensions of 9.25 mm diameter and 18 mm height. The foams were compression tested using a Instron 5501R Universal Testing Machine. Following the method used by Brezny and Green,[20] aluminium spacers of 9 mm diameter and 5 mm height were fixed to both the flat ends of the cylindrical samples so that load transfer to the samples was uniform. Furthermore, the static elastic modulus was estimated from slope of the elastic part of the stress–strain curve. Although the machine compliance has not been substracted, yet the estimated elastic modulus provides a useful comparison for the foams fabricated in this study, since the error is expected to be same for all the measurements.

3. Results and discussion

3.1. Effect of process variables

A slurry with near optimum composition of 32 vol.% solid loading, 4 vol.% PVA, 10 vol.% sucrose and 5 vol.% of colloidal silica (designated as the slurry A) has been used to study the effect of process parameters on its final structure.

3.1.1. Role of solid loading and binder content

The extent of solid loading and the binders controls the viscosity of the slurry formed. For a given level of binders in the aqueous slurry, viscosity increases with increase in the solid loading. Fig. 1 shows plots showing the variation of viscosity and shear stress with shear rate of the slurry A. All slurries have shown shear thinning (viscoelastic) behavior, very typical of such highly loaded slurries,[21] as is evident from Fig. 1. Such a behavior is critical for the processing methodology adopted, as it ensures that mixing and foaming operations occur during the low viscosity regime because of the shearing action associated with the ball-milling operation. Also, once the foam is cast in the subsequent step, there is no further movement or shearing action involved, and so the settling of the foam is inhibited because of the steep increase in viscosity. Based on this, a maximum solids loading of 32 vol.% was selected along with a binder system containing 4 vol.% PVA, 10 vol.% sucrose and 5 vol.% of colloidal silica for making the foams.

Table 1
Density and shrinkage data for silica foam panels obtained from mixture A (32 vol.% solid loading, 4 vol.% PVA, 10 vol.% sucrose and 5 vol.% of colloidal silica) foamed for 3 h

Green body characteristics	
Density (% theoretical)	10–15
Linear drying shrinkage (%)	10
Volume shrinkage (%)	23
Sintered body characteristics	
Density (%)	11
Sintering shrinkage (%)	Negligible

3.1.2. Effect of foaming time

The mixing process outlined above leads to the formation of bubbles in the slurry. Fig. 2 shows plots depicting the variation of green density and air inclusion volume with processing duration, which confirm that the volume of entrained air depends on the tumbling time (or foaming time). Further, Fig. 3 shows the plots depicting variation of the porosity content and weight of the panels, which were dried at 110 °C, as a function of foaming time. Examination of the plots in Fig. 3 indicates that the porosity content of the panels, estimated using the Archimedes principle, increases with the foaming time and levels off after about 3 h. On the other hand, the volume of a

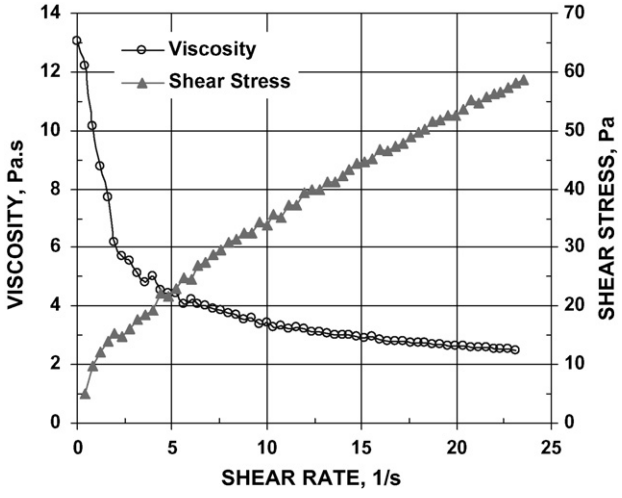

Fig. 1. Plots showing the variation of viscosity and shear stress with shear rate of the slurry.

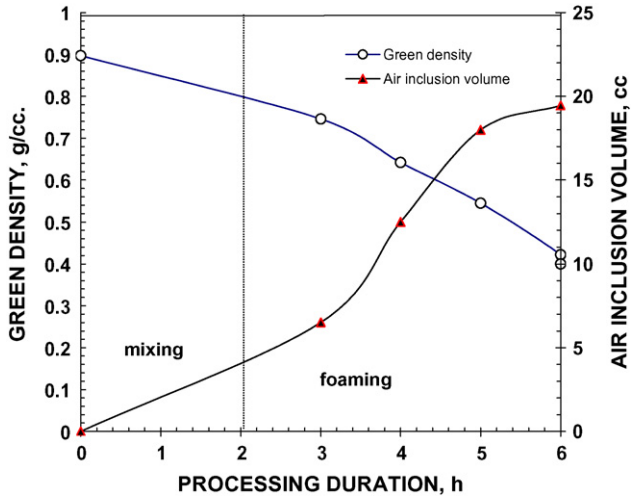

Fig. 2. Plots showing the variation of green density and air inclusion volume with the duration of processing.

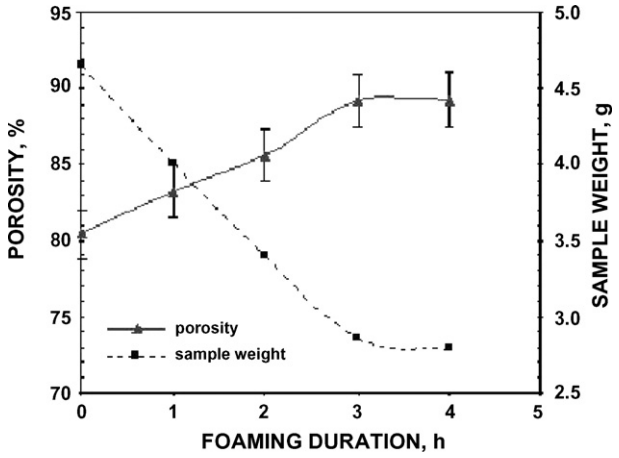

Fig. 3. Plots showing the variation of the porosity content and weight of samples dried at 110 °C, as a function of foaming time.

sample having a specified mass, increases till 3 h of foaming time, as expected from the results shown in Fig. 3. The regime of no change in porosity content is reached, once the foam is completely stabilized with the bubbles frozen in position, thus precluding further entrainment of air. In fact, the foams formed after 3 h can no longer be poured into a container; and those have to be scooped out like ice-cream with a spoon and transferred.

Fig. 4(a)–(d) presents optical micrographs of the vertical section of green samples corresponding to that after mixing, and 1, 2 and 3 h of foaming, respectively. It is possible to study the evolution of pore size distribution with foaming time in the optical images shown in Fig. 4(a)–(d). It has been found that the pores

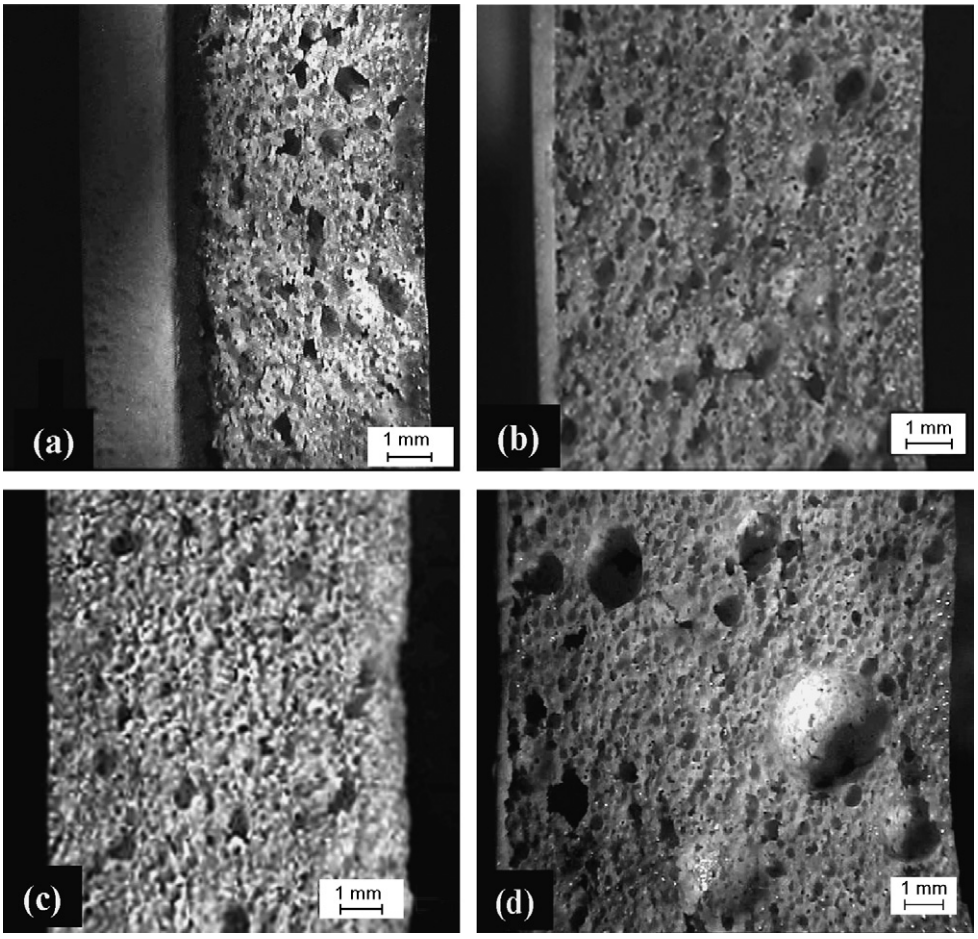

Fig. 4. Optical micrographs showing the effect of processing condition of foam stability and porosity after: (a) mixing, and (b) 1 h (c) 2 h and (d) 3 h of foaming.

Table 2
Composition and densities of foams, sintered at 1100 °C

Mixture designation	Mixture constitution (in vol.%)	Foaming time (h)	Relative density of sintered foam (%)
A	Solid 32%, PVA 4%, sucrose 10%, colloidal silica 5%	3	11
B	Solid 28%, PVA 4%, sucrose 10%	3	15
C	Solid 25%, PVA 4%, sucrose 10%	4	18
D	Solid 28%, PVA 4%, sucrose 10%	2	32
E	Solid 25%, PVA 4%, sucrose 10%, $AlPO_4$ 5%	2	62

are bigger, and the pore size distribution is inhomogenous in the samples subjected to foaming for more than 3 h. The inhomogeneous distribution of pores is perhaps due to the coalescence of smaller bubbles after 3 h of foaming. However, the panels made with foaming for less than 3 h (that is, just after mixing or after 1 or 2 h of foaming) have kinetically unstable bubbles, and also show a denser bottom layer due to drainage.

3.1.3. *Effect of drying*

The as-cast foam contains the same amount of water as the starting slurry. The water has to be removed by a drying step to prepare the green body for sintering afterwards at higher temperatures. Drying constitutes the longest, and the most critical part of the process. If it is carried out very fast or in an uncontrolled manner, the resulting shrinkage can lead to cracks in the dried panel. On the other hand, if the drying step is carried out very slowly, it could provide sufficient time for the smaller bubbles to coalesce and collapse. Hence it is important that drying should be carried out under well-controlled temperature and humidity conditions.

The plots of water content and drying rate against time are shown in Fig. 5. Water content in the sample is expressed as a fraction of the weight of the final dry solid, while the drying rate is represented as the net weight fraction of the water lost per unit time per unit cross sectional area of the container. The water content decreases with time at close to a linear rate. The rate of drying increases, only when ratio of the drying temperature to humidity is increased. The linear rate of drying is in sharp contrast to the normal trend of distinct zones of a constant rate drying period, followed by regions of falling rate periods, commonly observed during drying of a slurry.[21–23] This unusual behavior arises because of the structure of the pores in the cast foam. In a normal sample formed by the casting of a slurry, water occupies the interparticulate void regions, and removal of water during drying of such a sample follows the typical drying rate mechanisms described exhaustively in literature.[22,23] In contrast, in the cast foam, only the particulate network forming the cell walls of the structure holds the water, and the internal void space contains the air, entrained during processing to create porosity. In fact, the porous structure can be considered as a 3D network of spherical voids, which are interconnected with each other by the porosity as well as by punctures in the cell walls (structure of the foam is discussed in Section 3.4). Fig. 6(a) and (b) shows schematically the structures of a porous solid and a foam with interconnected porosities, respectively. Such interconnected porosities coupled with a very large pore volume (in excess of 80%) also provide a significantly large surface area for the water to evaporate and go out of the sample. The mechanism is therefore akin to the one corresponding to the falling rate period in conventional drying of particulate solids, and the observed rate of drying for a given temperature and humidity is proportional to the water content in the sample as shown in Fig. 5. This is further substantiated by the fact that even 25 mm thick panels could be dried without cracking with less than 10% shrinkage in its length.

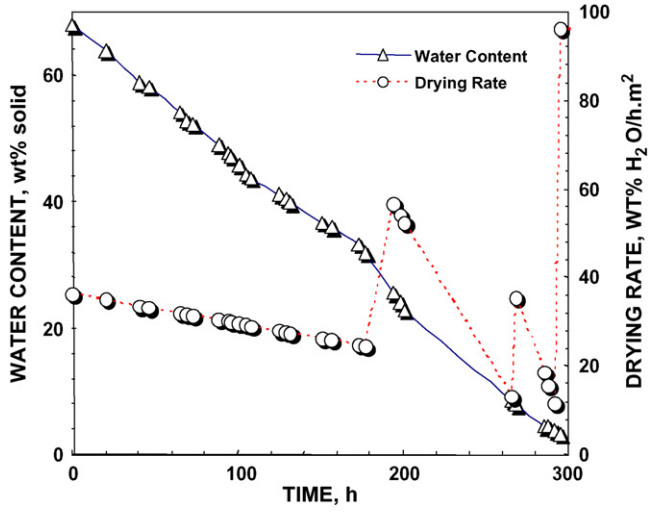

Fig. 5. Plots showing the kinetics of drying of the foam under controlled humidity conditions.

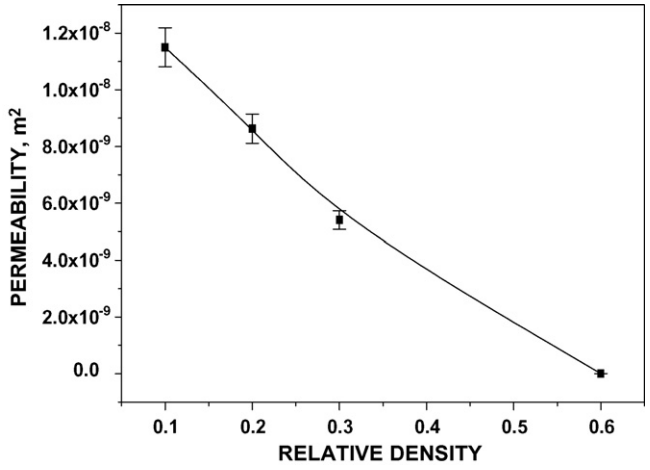

Fig. 6. Schematic diagram showing the structure of: (a) porous solid and (b) foam made from the drying of particulate slurries. In (a), the hatched region shows the spherical particles, and the white regions represent the interparticulate voids. In (b), the hatched regions depict the cell walls formed by the particles, and the white regions represent the spherical pores.

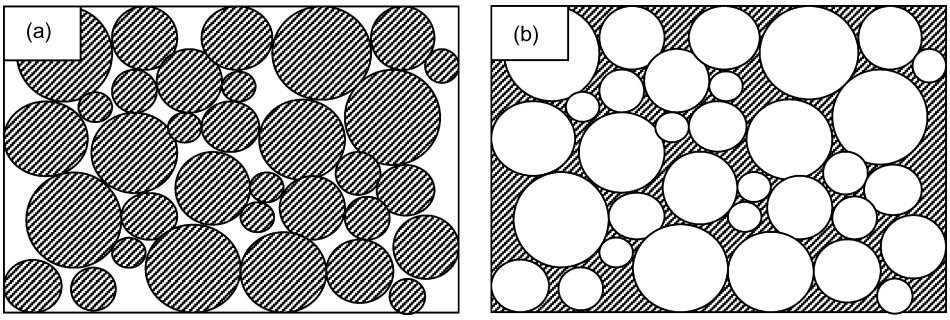

Fig. 7. Plot showing the variation of permeability of sintered bodies as a function of their relative density.

3.2. Physical characterization

3.2.1. Density

The density, porosity and volume shrinkage of the green and sintered tiles obtained from the slurry A foamed for 3 h, are listed in Table 1. Green density of the cast samples has been recorded as 0.248 ± 0.03 g/cc, while the density of sintered tiles has been found to be 0.368 ± 0.045 g/cc. Since the theoretical density is 2.25 g/cc, it is obvious that the porosities are preserved in the tiles after sintering. As mentioned earlier, density of the final foam is dependent on the solid loading, binder content, duration of foaming, drying and sintering. Table 2 shows the typical densities obtained in the foams, B, C, D and E, which have been prepared from slurries with different fractions of solid loading.

3.2.2. Permeability

For pore sizes below the millimeter range, the flow rate, Q is determined using the Darcy's relationship[24] shown in Eq. (1):

$$Q = \frac{K_D A \, \Delta P}{L \eta} \tag{1}$$

where ΔP is the pressure drop across a medium of length L, A is the cross-sectional area of sample, η is the viscosity of the flowing medium and K_D is the Darcy permeability coefficient. Any porous medium can be readily described by its relative density ρ/ρ_s, where ρ is the foam density and ρ_s is the theoretical density of the solid, that the foam is made of. The plot, showing the variation of permeability of the sintered foam samples

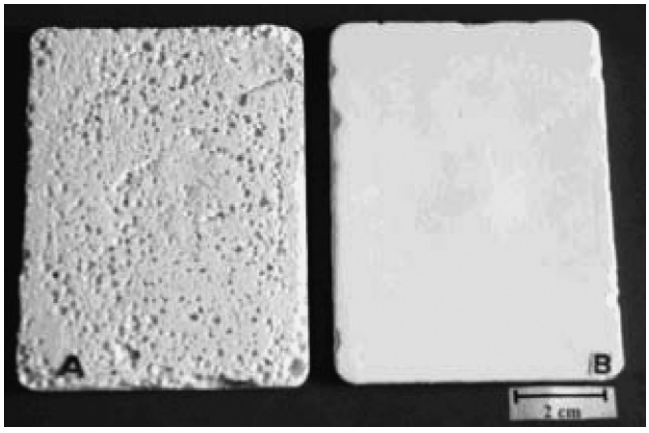

Fig. 8. Photographs of the green foam panels: (a) before and (b) after surface densification.

(25 mm × 25 mm × 8 mm) as a function of the relative density, is shown in Fig. 7. Examination of the results in Fig. 7 shows that the permeability decreases with the relative density of the porous body, as expected. For densities less than 30%, the permeability is $\sim 10^{-8}$ m^2, whereas for the samples with 60% density, it is further reduced to 10^{-12} m^2.

3.3. Surface densified foam panels

A coating having thickness in the range of 200–300 μm was applied for surface densification of some of the foams after the completion of drying to fill the bigger pores, improve

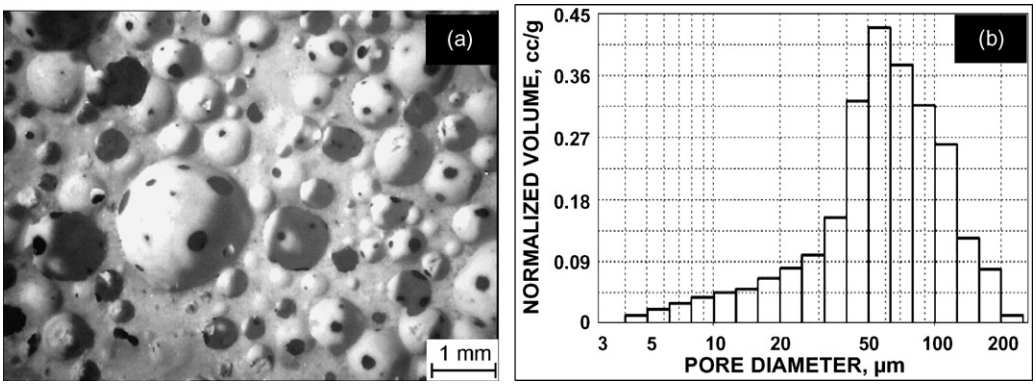

Fig. 9. (a) Typical optical micrograph of 15% dense silica foam, showing interconnected porosities and (b) pore size distribution for a sample with 89% porosity, determined by mercury intrusion porosimetry, showing a skewed broadband distribution of pores with an average pore size of ~70 μm.

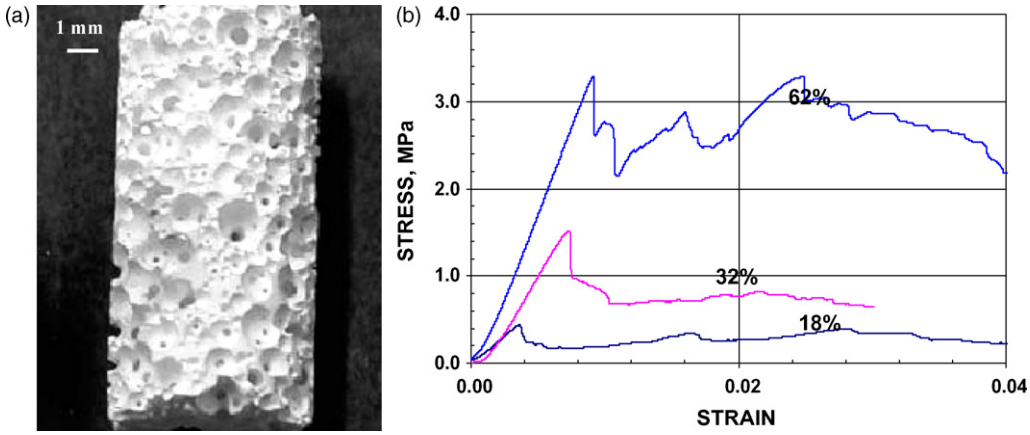

Fig. 10. Compression tests: (a) a typical sintered (9.25 mm diameter, 15 mm long) foam sample and (b) plots showing the variation of compressive stress with strain for the foam with densities in the range of 18–62%.

the smoothness, and make it resistant to wear. During sintering, thick or uneven coatings cracked. The green porous silica tiles before and after surface densification are shown in Fig. 8(a) and (b), respectively. The surface density has been found to be 0.797 g/cc (35% of the theoretical). Examination of the surfaces using optical microscopy has confirmed the presence of a uniform distribution of micropores of 30–50 μm size.

3.4. Microstructure

Fig. 9(a) shows a typical optical micrograph of the 15% dense (measured using Archemedes principle) silica foam, made from the slurry, B. The microstructure clearly indicates that the pores are generally spherical, with open and interconnected porosity. Using image analysis by point counting method, the pore volume fraction has been measured as 73.3% ± 1.3. The discrepancy between the expected porosity level of 85% and the experimentally determined pore volume fraction of 73.3% is attributed to the presence of micropores with sizes less than the resolution limit of the optical microscope. The surface area per unit volume determined through the linear intercept method is 28.3 cm^2/cc, which is suggestive of an average pore size of ~200 μm. Results of mercury intrusion porosimetry, shown in Fig. 9(b), however suggests a relatively smaller average size of ~70 μm, with a predominance of pores in the range of 40–200 μm sizes. The difference between the results of image analysis and mercury porosimetry is attributed to the interconnections between the pores. If a bigger pore is filled through a smaller channel or pore, the pressure requirement will be higher than when the bigger pore is filled directly. Hence the data will get skewed towards the lower side (filling of a bigger pore but at higher pressure), while in reality the pore size is larger than what is measured.

3.5. Mechanical behavior

Sintered silica foams obtained from further processing of the slurries, C, D and E (Table 2), and having 18%, 32% and 62% of theoretical density, respectively have been evaluated for their compressive strength at ambient temperatures. Fig. 10(a) and (b) show respectively, the photograph of a typical test sample, and a collection of plots of stress against strain for porosity. All the samples exhibit mechanical behavior, typical of cellular materials. The compressive stress shows an initial linear elastic region, followed by a drop indicating cracking of the sample. Subsequently, further strain leads to the collapse of some part of the structure, while the other parts support against the applied load leading to increase in the stress against displacement (Fig. 10). As all the cell walls collapse, and begin to press against each other, the stress is expected to increase again. The plots showing the variation of peak compressive stress, and the estimated static elastic modulus values of the foams with their density are presented in Fig. 11. As expected, both the yield stress and elastic modulus increase with relative density. The static elastic modulus increases from 120 MPa to 390 MPa and compressive strength increases from 0.45 MPa to 3.30 MPa, on increasing the relative density from 18% to 62%. The optical micrographs of the fractured foam surfaces are shown in Fig. 12. It is clear that failure has occurred at an angle to the applied stress axis,

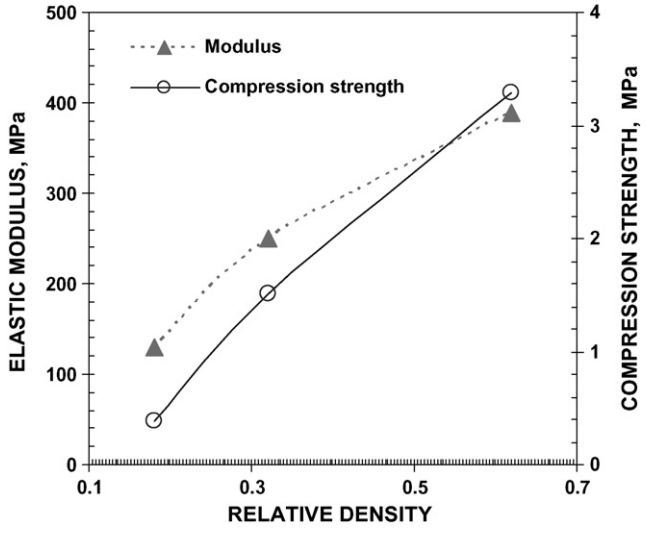

Fig. 11. Plots showing the variation of elastic modulus and compressive strength of the foams as a function of their relative density.

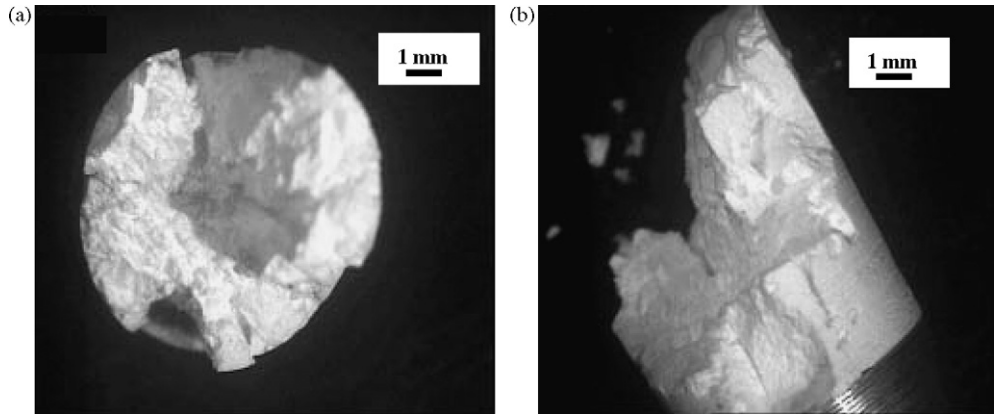

Fig. 12. Optical micrographs of the fractured surfaces of silica foams being viewed from: (a) the top and (b) the side.

indicating the role of shear. Brittle materials are strong in compression but weak in shear, and usually undergo failure under compressive stress along the plane of maximum shear.

4. Summary

A novel approach for producing the ceramic foams from inexpensive silica powder has been developed. The pores produced with this approach, result from the direct entrainment of air bubbles into a ceramic suspension. The different processing parameters that control the final properties of foams have been optimized. Panels with thickness of 25 mm have been dried in a controlled manner without cracking, and with uniform linear shrinkage of 10%. Silica foams having high structural integrity, nearly spherical pores with average size of ∼2 mm, interconnected porosity, and possessing as low as 11% of the theoretical density, have been successfully fabricated. The permeability, elastic modulus and the compressive strength of the porous silica tiles are a function of the foam density. The silica foams thus produced, have strength levels in the range of ∼0.5 MPa to 3.3 MPa, for densities in the range of 18–62%. A surface densification process for the porous tiles, that can partially seal off the relatively larger surface pores, as well as provide a smooth exterior and adequate strength for protection against mass loss during handling has also been established.

Acknowledgement

The authors are thankful to Director, DMRL for his encouragement and support.

References

[1]. Sepulveda, P., Gelcasting foams for porous ceramics. *Am. Ceram. Soc. Bull.*, 1997, **76**(10), 61–65.
[2]. Saggio-Woyansky, J., Scott, C. E. and Minnear, W. P., Processing of porous ceramics. *Am. Ceram. Soc. Bull.*, 1992, **71**(11), 1674–1682.
[3]. Sundermann, E. and Viedt, J., Method of manufacturing Ceramic foam bodies. U.S. Pat. No. 3 745 201, 10 July 1973.
[4]. Wood, L. L., Messina, P. and Frisch, K., Method of preparing porous ceramic structures by firing a polyurethane foam that is impregnated with organic material. U.S. Pat. No. 3 833 386, 3 September 1974.
[5]. Motoki, H., Process for preparing a foamed body. U.S. Pat. No. 4 084 980, 18 April 1978.
[6]. Jackson, G. and Meredith, W., Inorganic foams. U.S. Pat. No. 4 547 469, 15 October 1985.
[7]. Helferich, R. L. and Schenck, R. C., Process for producing porous ceramic filters for filtering of particulates from diesel engine exhaust gases. U.S. Pat. No. 4 871 485, 3 October 1989.
[8]. Minnear, W. P., Processing of foam ceramics. In *Forming Science and Technology for Ceramics*, ed. M. J. Cima. American Ceramic Society, Westerville, 1992, pp. 146–156.
[9]. Peng, H. X., Fan, Z., Evans, J. R. G. and Busfield, J. J. C., Microstructure of ceramic foams. *J. Eur. Ceram. Soc.*, 2000, **20**(7), 807–813.
[10]. Peng, H. X., Fan, Z. and Evans, J. R. G., Cellular arrays of alumina fibres. *J. Mater. Sci.*, 2001, **36**(4), 1007–1013.
[11]. Powell, S. J. and Evans, J. R. G., The structure of ceramic foams prepared from polyurethane–ceramic suspensions. *Mater. Manuf. Process.*, 1995, **10**(4), 757–771.
[12]. Colombo, P. and Hellmann, J. R., Ceramic foams from preceramic polymers. *Mater. Res. Innov.*, 2002, **6**(5–6), 260–272.
[13]. Colombo, P. and Bernardo, E., Macro- and micro-cellular porous ceramics from preceramic polymers. *Compos. Sci. Technol.*, 2003, **63**(16), 2353–2359.
[14]. Takahashi, T., Munstedt, H., Colombo, P. and Modesti, M., Thermal evolution of a silicone resin/polyurethane blend from preceramic to ceramic foam. *J. Mater. Sci.*, 2001, **36**(7), 1627–1639.
[15]. Studart, A. R., Gonzenbach, Urs, T., Tervoort, E. and Gauckler, L. J., Processing routes to macroporous ceramics: a review. *J. Am. Ceram. Soc.*, 2006, **89**(6), 1771.
[16]. Du, Z. P., Bilbao-Montoya, M. P., Binks, B. P., Dickinson, E., Ettelaie, R. and Murray, B. S., Outstanding stability of particle-stabilized bubbles. *Langmuir*, 2003, **19**(8), 3106–3108.
[17]. Dickinson, E., Ettelaie, R., Kostakis, T. and Murray, B. S., Factors controlling the formation and stability of air bubbles stabilized by partially hydrophobic silica nanoparticles. *Langmuir*, 2004, **20**(20), 8517–8525.
[18]. Binks, B. P. and Horozov, T. S., Aqueous foams stabilized solely by silica nanoparticles. *Angewandte Chemie—Int. Ed.*, 2005, **44**(24), 3722–3725.
[19]. Gonzenbach, U. T., Studart, A. R., Tervoort, E. and Gauckler, L. J., Ultrastable particle-stabilized foams. *Angewandte Chemie—Int. Ed.*, 2006, **118**, 3606–3610.
[20]. Brezny, R. and Green, D. J., Uniaxial strength behavior of brittle cellular materials. *J. Am. Ceram. Soc.*, 1993, **76**(9), 2185–2192.
[21]. Reed, J. S., *Principles of Ceramic Processing* (*2nd ed.*). John Wiley and Sons, Inc, New York, 1988, p. 283.
[22]. Geankoplis and Christie, J., *Transport Processes & Unit Operations* (*3rd ed.*). Prantice Hall of India Pvt. Ltd, New Delhi, 2000, p. 536.
[23]. Rahaman, M. N., *Ceramic Processing and Sintering*. Marcel Dekker, Inc, New York, 1988, pp. 220–230.
[24]. Scheidegger, A. E., *The Physics of flow through porous media*. University of Toronto Press, Toronto, Canada, 1974, Chapters 4, 7.